LANGMUIR Article
Cite This: Langmuir 2018, 34, 7309−7318
pubs.acs.org/Langmuir

The Nucleation Rate of Single O_2 Nanobubbles at Pt Nanoelectrodes

Álvaro Moreno Soto,*[,†,‡] Sean R. German,[†] Hang Ren,[†] Devaraj van der Meer,[‡] Detlef Lohse,*[,‡] Martin A. Edwards,[†] and Henry S. White*[,†]

[†]Department of Chemistry, University of Utah, 315 South 1400 East, Salt Lake City, Utah 84112-0850, United States
[‡]Physics of Fluids Group and Max Planck Center Twente, MESA+ Institute and J. M. Burgers Centre for Fluid Dynamics, Faculty of Science and Technology, University of Twente, P.O. Box 217, 7500 AE Enschede, The Netherlands

Supporting Information

ABSTRACT: Nanobubble nucleation is a problem that affects efficiency in electrocatalytic reactions since those bubbles can block the surface of the catalytic sites. In this article, we focus on the nucleation rate of O_2 nanobubbles resulting from the electrooxidation of H_2O_2 at Pt disk nanoelectrodes. Bubbles form almost instantaneously when a critical peak current, i_{nb}^{p}, is applied, but for lower currents, bubble nucleation is a stochastic process in which the nucleation (induction) time, t_{ind}, dramatically decreases as the applied current approaches i_{nb}^{p}, a consequence of the local supersaturation level, ζ, increasing at high currents. Here, by applying different currents below i_{nb}^{p}, nanobubbles take some time to nucleate and block the surface of the Pt electrode at which the reaction occurs, providing a means to measure the stochastic t_{ind}. We study in detail the different conditions in which nanobubbles appear, concluding that the electrode surface needs to be preconditioned to achieve reproducible results. We also measure the activation energy for bubble nucleation, E_a, which varies in the range from (6 to 30)kT, and assuming a spherically cap-shaped nanobubble nucleus, we determine the footprint diameter L = 8−15 nm, the contact angle to the electrode surface θ = 135−155°, and the number of O_2 molecules contained in the nucleus (50 to 900 molecules).

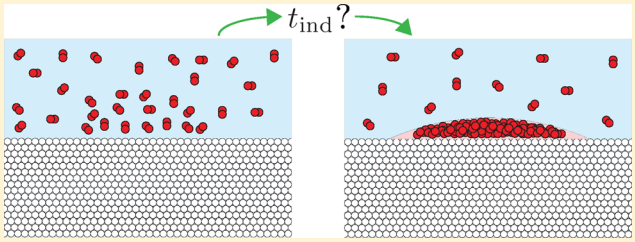

INTRODUCTION

The generation of bubbles in chemical reactions is a process that has been well known by scientists throughout history. When these bubbles are extremely small (on the order of nanometers), the problem becomes much more challenging to analyze.[1−3] However, the technology used to visualize such surface nanobubbles has been very recently developed.[2,4−6] The biggest concern that surface nanobubbles cause is their generation in chemical reactions, such as electrolysis[7] and catalysis.[8] Nanobubbles nucleating on top of reacting surfaces or electrodes influence the efficiency of chemical reactions since they partially block the reactive surface and consequently impede the reaction of interest.[9] A similar situation occurs in the case of nanodroplet and nanocrystal nucleation.[10] In other scenarios, such as redox reactions in cells, the nanobubbles can form within the nanoprobes and induce current amplification.[11] The high internal pressures of nanobubbles make their behavior rather different from that of micro- or macrobubbles.[2,12] Nanobubbles often adhere to the surface at which they originate, forming a spherical cap that strongly attaches to the active surface.[2,13] Without pinning, i.e., when the nanobubbles are not attached to a specific location on the surface, due to the high pressure inside them,[14,15] nanobubbles would dissolve extremely rapidly once the reaction stops. However, if there are pinning sites and constant gas supersaturation is provided at the surface, then nanobubbles on reacting surfaces are very stable[16,17] and do not dissolve.[2] Molecular dynamics simulations[18] support this view.

In this article, we measure the nucleation rate of single O_2 nanobubbles generated at Pt nanodisk electrodes by the electro-oxidation of H_2O_2. When the local dissolved O_2 concentration at the nanoelectrode is sufficiently high,[19] a nanobubble nucleates and blocks the reacting surface, as depicted in Figure 1. We study the factors affecting the nucleation rate of O_2 nanobubbles under different applied currents.

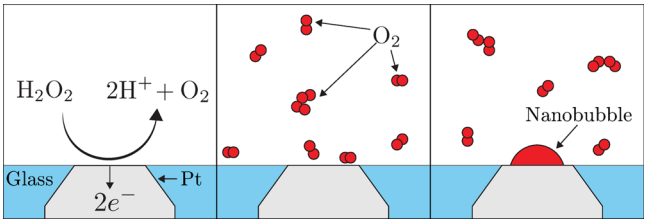

Figure 1. O_2 nanobubble generation by electro-oxidation of H_2O_2. When the O_2 concentration at the nanoelectrode is sufficiently high, a nanobubble nucleates after some time and partially blocks the electrode surface.

Received: April 26, 2018
Revised: May 25, 2018
Published: May 30, 2018

DOI: 10.1021/acs.langmuir.8b01372
Langmuir 2018, 34, 7309−7318

EXPERIMENTAL METHODS

The fabrication and measurement of the size of Pt nanoelectrodes are described in detail in the Supporting Information (section 1). All experiments were performed in an aqueous solution of 1 M H_2O_2 and 1 M $HClO_4$, prepared using purified deionized water (18.2 MΩ·cm).

A HEKA EPC10 patch clamp amplifier was used to collect current, i, voltage, E, and time, t, data, which were filtered with a 4-pole Bessel low-pass filter at 10 kHz and sampled at 50 kHz. A LabVIEW program employing a FPGA card (National Instruments, PCIe-7852) was used to monitor the voltage and to control current steps for galvanostatic experiments. The program was capable of lowering the current to 0 nA within 80 μs after the detection of nanobubble nucleation. A mercury sulfate electrode (BASi) was employed (E = +0.64 V relative to a normal hydrogen electrode, NHE) as a reference/counter electrode in a two-electrode configuration. For convenience, all potentials are presented vs NHE.

RESULTS AND DISCUSSION

Cyclic Voltammogram in a Solution of 1 M H_2O_2 and 1 M $HClO_4$. The generation of a single nanobubble at a Pt nanoelectrode can be observed in cyclic voltammetric measurements, as reported in previous work.[20,21] Figure 2 shows the cyclic voltammogram of a 6-nm-radius electrode in an aqueous solution of 1 M H_2O_2 and 1 M $HClO_4$.

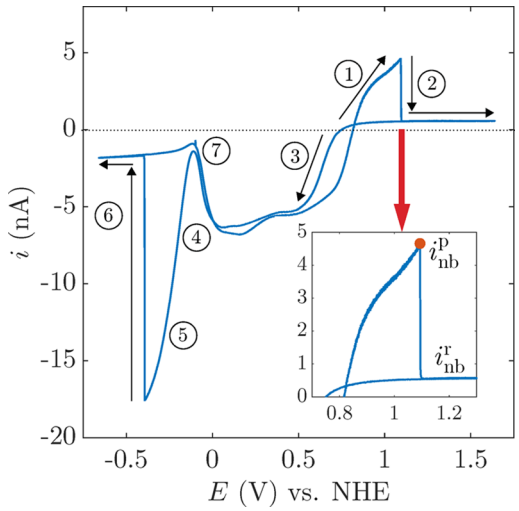

Figure 2. Cyclic voltammogram of a 6-nm-radius Pt nanoelectrode in a solution of 1 M H_2O_2 and 1 M $HClO_4$. The red dot on the close-up area corresponds to the peak current i^p_{nb} at which a nanobubble nucleates and then grows to block the electrode surface. The scan rate is 200 mV/s.

The i–E response reflects several potential-dependent electrochemical reactions,[21] as labeled in Figure 2:

1. $H_2O_2 \rightarrow 2H^+ + 2e^- + O_2$: above 0.8 V, H_2O_2 is electrochemically oxidized to produce dissolved O_2. The higher the current, the faster the rate of O_2 production and the higher the local supersaturation.[19]
2. O_2 nanobubble formation: when the current reaches the peak value, i^p_{nb}, the concentration of O_2 is sufficiently high that a nanobubble nucleates at the nanoelectrode, grows, and blocks it, as depicted in Figure 1. Consequently, the current rapidly drops to a residual current, i^r_{nb}, which corresponds to the balance of the steady-state O_2 dissolution from the bubble to the bulk with the O_2 production at the circumference of the nanoelectrode (which is not fully covered by the nanobubble).[20,22] Increasing the voltage from that point on causes no change in the current, which remains constant at i^r_{nb}.[20] This current also stays constant when we subsequently reduce the voltage until O_2 electrogeneration ceases and the nanobubble dissolves.
3. $H_2O_2 + 2e^- + 2H^+ \rightarrow 2H_2O$: from 0.8 to 0 V, H_2O_2 is reduced to form H_2O, resulting in a cathodic current.
4. $H^+ + e^- \rightarrow$ Pt–H: a monolayer of H· is reductively adsorbed at the Pt surface,[23] reducing the rate of H_2O_2 reduction, resulting in a decrease in the cathodic current.
5. $2H^+ + 2e^- \rightarrow H_2$: from −0.1 to −0.4 V, protons are reduced to produce H_2.
6. H_2 nanobubble formation: when enough H_2 molecules cluster together, a H_2 nanobubble nucleates at the nanoelectrode, as indicated by a sudden decrease in current to a potential-independent residual current.
7. As the electrode potential is scanned toward positive voltages (from 0 to 0.8 V), H desorbs from the Pt and the rate of H_2O_2 reduction increases.

This cyclic voltammogram may be scanned hundreds of times, with repeated formation and dissolution of the O_2 and H_2 nanobubbles on each scan.[24] However, large variability in i^p_{nb} is observed after an extensive repetition of voltammetric cycles. This is likely due to the restructuring of the surface in the repetitive scans, as the voltammetric responses involve H· absorption and desorption (from 0 to 0.8 V, steps 3 and 7 in Figure 2) and the oxidation and reduction of H_2O_2 involve the generation of PtO_x as well as the reduction of PtO_x to Pt.[23] However, the self-decomposition of H_2O_2 to O_2 caused by the Pt surface[25,26] does not play a significant role in the case of eventual bubble nucleation since the O_2 generation rate is negligible compared to the gas production rate once a certain current is applied.[21] The electrode apparent radius a is also affected during the application of the conditioning cycles (section 1 in the Supporting Information); consequently, i^p_{nb} may be affected.[21,22,27] Figure 3 shows several cyclic voltammograms recorded at the same electrode, displaying a different i^p_{nb} in every cycle. However, by reducing the scan range or applying

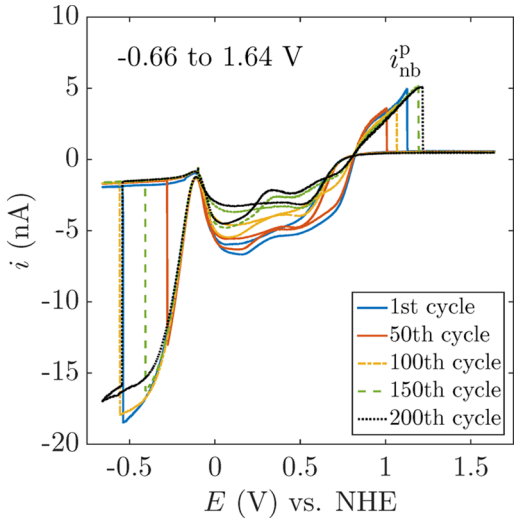

Figure 3. Multiple voltammetric cycles demonstrating the generation of O_2 and H_2 nanobubbles. Note that the curves show a large variation. More specifically, the current i^p_{nb} at which an O_2 nanobubble forms varies significantly from cycle to cycle. The voltammograms were recorded at a 6-nm-radius electrode at a scan rate of 200 mV/s.

DOI: 10.1021/acs.langmuir.8b01372
Langmuir 2018, 34, 7309−7318

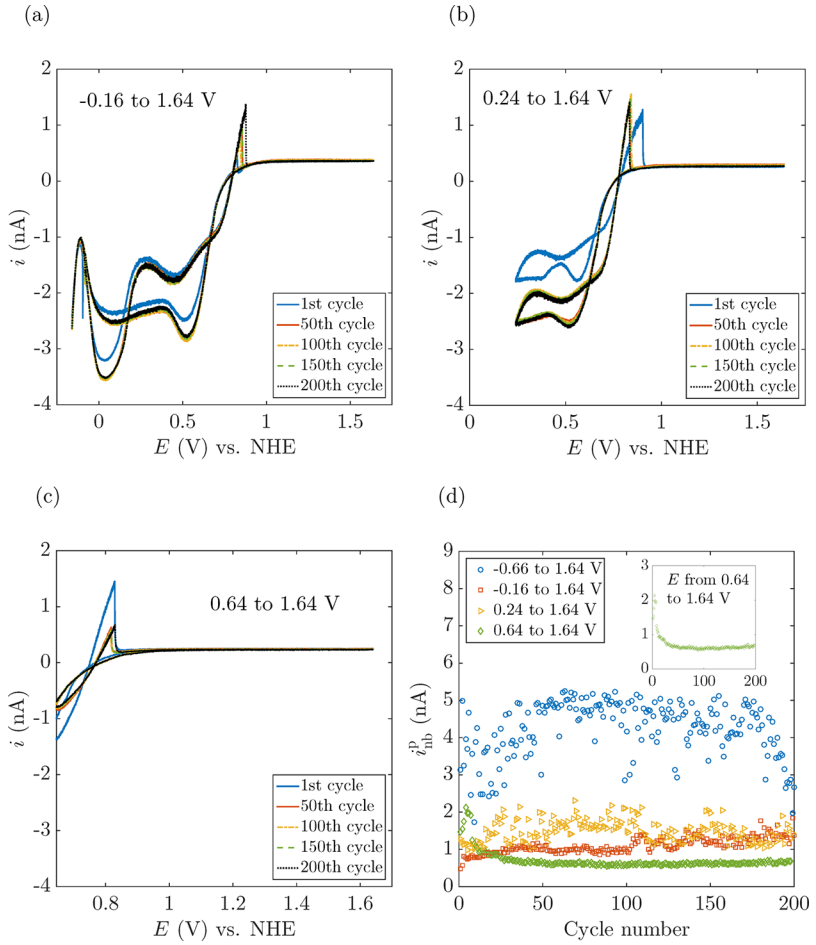

Figure 4. (a–c) Multiple cycles of voltammograms performed over different potential scan ranges for the determination of experimental conditions giving rise to reproducible i_{nb}^{P} for O_2 nanobubble formation on a 6-nm-radius electrode. (d) i_{nb}^{P} vs cycle number for O_2 nanobubble formation for different scan ranges corresponding to voltammograms in panels a–c and Figure 3. The voltammetric cycle shown in panel (c) is the one that involves the least surface chemistry and thus, results in the most reproducible results (green diamonds in panel (d)). Note that the mean value of i_{nb}^{P} changes for different scan ranges, again highlighting the importance of the surface chemistry.

a "conditioning cycle", a reproducible electrode surface and a constant apparent radius, and therefore a consistent i_{nb}^{P}, can be achieved. We can thus influence the surface chemistry of the Pt electrode, achieving a more reproducible i_{nb}^{P}.[28] Figure 4 presents several voltammograms of the same electrode covering different scan ranges, with the resulting variability of i_{nb}^{P} shown in Figure 4d. It is important to notice the different mean values of i_{nb}^{P} for different scan ranges, which emphasizes the importance of the surface chemistry on bubble nucleation.

Once we have secured a reproducible i_{nb}^{P}, we can turn to the objective of our story: the measurement of the different rates at which nanobubbles nucleate if a certain current below i_{nb}^{P} is applied.

Measurement of the Nucleation Rate. Our experiments aim at measuring the time to nucleate a nanobubble as a function of the applied current i_{app}. In the experiments described above, the nanobubbles nucleate "instantaneously" on the voltammetric time scale when the current reaches i_{nb}^{P} (which is approximately linearly related to the electrode apparent measurable radius a[21,22]). However, if i_{app} is lower than i_{nb}^{P}, then a measurable stochastic induction time is required for nucleation.[21]

As shown in Figure 4d, at least 40 cycles need to be performed before a good i_{nb}^{P} reproducibility is reached. Therefore, we designed the conditioning cycle shown in Figure 5a to obtain reproducible results during the nucleation rate experiments. First, the voltage is swept positively until an O_2 nanobubble nucleates and blocks the electrode. The voltage is then stepped to E = 0.64 V for a defined time, t_{dis}, to allow the nanobubble to dissolve; this dissolution is followed by a stabilization process in which the electrode surface is conditioned by holding it at a voltage, E_{stab}, for a time, t_{stab}. Finally, we let the electrode rest at E = 0.64 V for a time t_{rest} before repeating the cycle. Conditioning waveforms using different combinations of t_{dis}, t_{stab}, E_{stab}, and t_{rest} have been experimentally tried and are presented in the table in Figure 5c. The optimized conditions correspond to t_{dis} = 1 s, t_{stab} = 2 s, E_{stab} = 0.89 V, and t_{rest} = 1 s, corresponding to conditioning protocol #4 (green diamonds) in Figure 5b, where we represent i_{nb}^{P} vs the cycle number corresponding to the most representative data among 20 different conditioning configurations. The different i–E vs t plots of these conditioning cycles have been included in the Supporting Information (Figure S4).

Now we can measure the nucleation rate at different supersaturation levels, which are directly controlled by the applied current.[29] We chose to control current rather than voltage because the experiment is very sensitive to any drift in

DOI: 10.1021/acs.langmuir.8b01372
Langmuir 2018, 34, 7309–7318

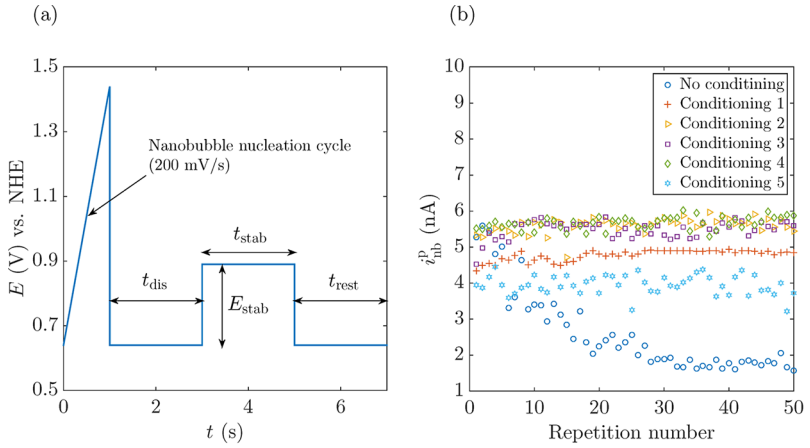

(c)

Conditioning # in Figure 5b (symbol)	t_{dis} (s)	t_{stab} (s)	E_{stab} (V)	t_{rest} (s)
No conditioning (blue ◯)	0	0	N/A	0
1 (red +)	2	0	N/A	0
2 (yellow ▷)	2	0	N/A	0
3 (purple □)	1	2	0.69	1
4 (green ◇)	1	2	0.89	1
5 (cyan ⋆)	1.5	3	0.89	10

Figure 5. (a) Voltammetric electrode conditioning cycle used to rapidly achieve a state where the O_2 nanobubble forms at a consistent current. (b) i^{P}_{nb} for the most representative combinations of t_{dis}, t_{stab}, E_{stab}, and t_{rest} as indicated in the table in panel (c). The configuration with the smallest standard deviation used throughout this article corresponds to configuration 4, with t_{dis} = 1 s, t_{stab} = 2 s, E_{stab} = 0.89 V, and t_{rest} = 1 s. (c) Table with the different configurations for conditioning the electrode to obtain reproducible results. The configuration which achieves the lowest standard deviation is highlighted in blue (diamond symbol) and is used in the remainder of the article and is referred to as "the electrode conditioning cycle".

the voltage. For example, in the region very close to i^{P}_{nb}, a change of 20 mV generated a change of 8% in current, as can be seen in Figure 6a, in which we plot a voltammogram for O_2 nanobubble nucleation. Such an apparent "small variation" in current causes a significant variation in the nucleation rate of nanobubbles. Control of the voltage is difficult to achieve with the desired precision. Therefore, we decided to control the current, which can be precisely adjusted to the level of pA.

A LabVIEW script was used to control the current i_{app} applied to the electrode. By subsequent step increases from $\sim 0.7 i^{P}_{nb}$ to $\sim 1.0 i^{P}_{nb}$, we can measure different nucleation times, which become smaller the closer i_{app} is to i^{P}_{nb}. The applied current loop is represented in Figure 6c, in which i_{stab} corresponds to the current response obtained during the application of E_{stab} in the course of electrode conditioning (Figure 5a). Once a nanobubble forms, according to the voltammogram presented in Figure 6a, if i_{app} is maintained fixed at a certain value, then the voltage will dramatically increase to values that correspond to water oxidation, damaging the nanoelectrode. Therefore, a threshold voltage E_{thres} = 1.5 V is established, so when a nanobubble nucleates and the voltage spikes, i_{app} will automatically return to zero.

We design a full experiment as shown in the flowchart of Figure 6b. First, the electrode surface is conditioned by applying the cycle in Figure 5a over a hundred times with voltage control. Afterward, we switched to current control, applying a fixed i_{app} until a nanobubble nucleates and blocks the electrode, while measuring the corresponding nucleation time t_{ind}. For the purpose of avoiding electrode surface reconditioning, if no bubble nucleated after 30 s, the current was manually set to zero and the process continued as designed. We repeated this loop for different currents 10 times before conditioning the electrode surface again. Several voltage responses are shown for a 41-nm-radius electrode corresponding to different i_{app} values in Figure 7 (see more results for different currents and different electrodes in the Supporting Information, Figures S5–S7). It can be perfectly appreciated that the closer i_{app} is to i^{P}_{nb}, the shorter t_{ind} becomes, e.g., $t_{ind} \approx 15$ s at i_{app} = 11.3 nA (Figure 7a), whereas when i_{app} is increased by 0.8 nA, t_{ind} drastically decreases to ~7 ms (Figure 7d). An increase of 7% in i_{app} causes a decrease in the nucleation time of 3 orders of magnitude. We report the different nucleation times t_{ind} for different i_{app} values on an a = 41 nm electrode in Figure 8a (refer to the Supporting Information, Figures S8 and S9, for the results corresponding to the different electrodes used in Figures S6 and S7). The stochasticity of the process can be appreciated in the different nucleation times measured at the same i_{app}. Notably, the closer i_{app} is to i^{P}_{nb} (i^{P}_{nb} = 12.2 nA for this case), the lower the variability of t_{ind}, i.e., the curves for different repetitions lie closer together. This effect originates from the shorter exposure time to a certain i_{app}, thus avoiding any reconditioning of the electrode surface. The shorter the exposure, the less the surface chemistry and consequently the more reproducible the results. For values of i^{P}_{nb} of approximately $0.9 i^{P}_{nb}$, the stochastic variability in t_{ind} ranges over 2 to 3 orders of magnitude,[29] moving toward values with variability within 1 order of magnitude for $0.99 i^{P}_{nb}$.

The cumulative probability of a nanobubble nucleating at a nanoelectrode can be expressed as $P = N(t)/N_T$, where $N(t)$ represents the number of nanobubbles whose nucleation occurs before a specific time t and N_T is the total number of nucleation events recorded at a certain i_{app}.[30] This cumulative probability can be theoretically expressed by an exponential relationship:[30,31]

$$P = 1 - e^{-J(t - t_{limit})} \quad (1)$$

DOI: 10.1021/acs.langmuir.8b01372
Langmuir 2018, 34, 7309–7318

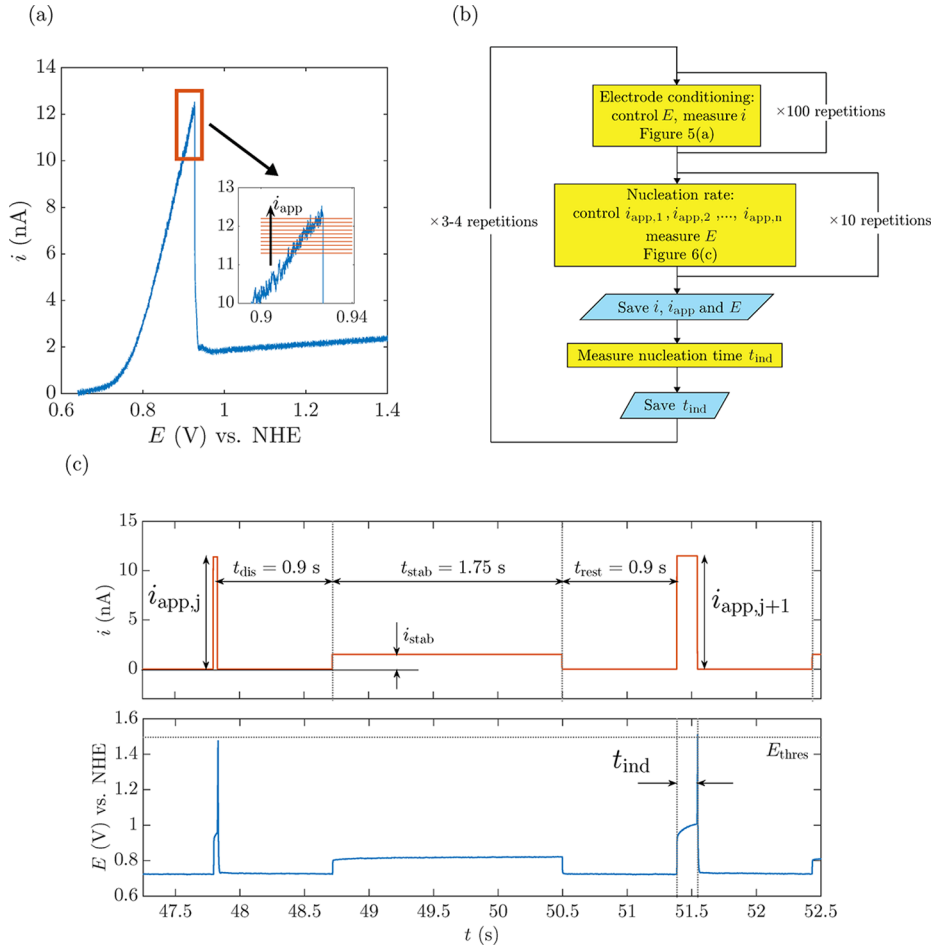

Figure 6. (a) Forward scan of a voltammogram for bubble formation at a 41-nm-radius Pt electrode. Inset: the range of i_{app} where bubble nucleation times are measured. (b) Experimental sequence used to determine bubble nucleation time as a function of i_{app}. (c) Applied current cycle (top) and measured potential (bottom) for determining the bubble nucleation time at the same electrode as in panel (a). The different times are defined similarly to the intervals in Figure 5a, whereas i_{stab} is the measured value of the current obtained during the application of E_{stab} in the same figure.

where J refers to the nucleation rate at a specific current and t_{limit} is the shortest accessible experimental time, which can be physically associated with the response time of the electronic circuit coupled to the capacitance of the electrochemical cell[29] and determines the minimum experimentally achievable t_{ind}. By fitting eq 1 to the data in Figure 8a, the nucleation rate, J, for each value of i_{app} can be measured as a best-fitting parameter. An estimate can be calculated as $J \approx 1/(\overline{t}_{ind} - t_{limit})$, where $\overline{t}_{ind}$ is the mean value of the nucleation time at a certain i_{app}. A single value of t_{limit} was fit to all measurements with each electrode. The probability distribution for the different i_{app} values in Figure 8a is represented in Figure 8b. The best match between the fits and experiments occurs for intermediate levels of i_{app} since for the lower values, nanobubbles take a longer time to nucleate and therefore the nanoelectrode surface can be reconditioned to a different state, whereas for i_{app} very close to i_{nb}^{P} the process is so fast that any uncertainty in t_{limit} may result in a very significant uncertainty in J.

The nucleation rate, J, depends on i_{app}, increasing its value as i_{app} increases, as can be depicted from the more vertical sigmoidal curves in Figure 8b for higher values of i_{app}. From Classical Nucleation Theory (CNT), the nucleation rate of a nanobubble at the surface of the electrode can be expressed as[9,12,16,32,33]

$$J = J_0 e^{-16\pi\gamma^3\phi(\theta)/3kT(P_s-P_0)^2} \quad (2)$$

where J_0 is the pre-exponential factor which describes the statistical molecule-by-molecule process of nucleus growth (which can be considered to be constant with respect to i), γ is the surface tension of the gas−liquid interface (variations in the surface tension at molecular length scale, which have been shown to be minimal down to 10 nm,[20] are not considered), $\phi(\theta) = (1 + \cos(\theta))^2(2 - \cos(\theta))/4$ is a geometric function which depends on the nanobubble contact angle θ to the electrode surface[24,34,35] (which implicitly accounts for the minute effect of the surface tension between the electrode and the bubble[36]), $kT = 4.11 \times 10^{-21}$ J is the product of Boltzmann constant k and thermodynamics temperature $T = 298$ K, and P_s and P_0 refer to the pressure in the bubble and the ambient pressure in the bulk liquid, respectively. Note again that in the derivation of eq 2 a spherical cap shape of the bubble nucleus has been assumed. Once van der Waals forces and thus the disjoining pressure play a role, this is no longer the case and the nanobubble shape may differ from that of a perfect spherical cap.[37] Given the nanometric size of the bubbles, these considerations may apply. These deviations from a perfect spherical-cap shape are nevertheless known to be very small,[37] so our assumption may still be valid.

DOI: 10.1021/acs.langmuir.8b01372
Langmuir 2018, 34, 7309−7318

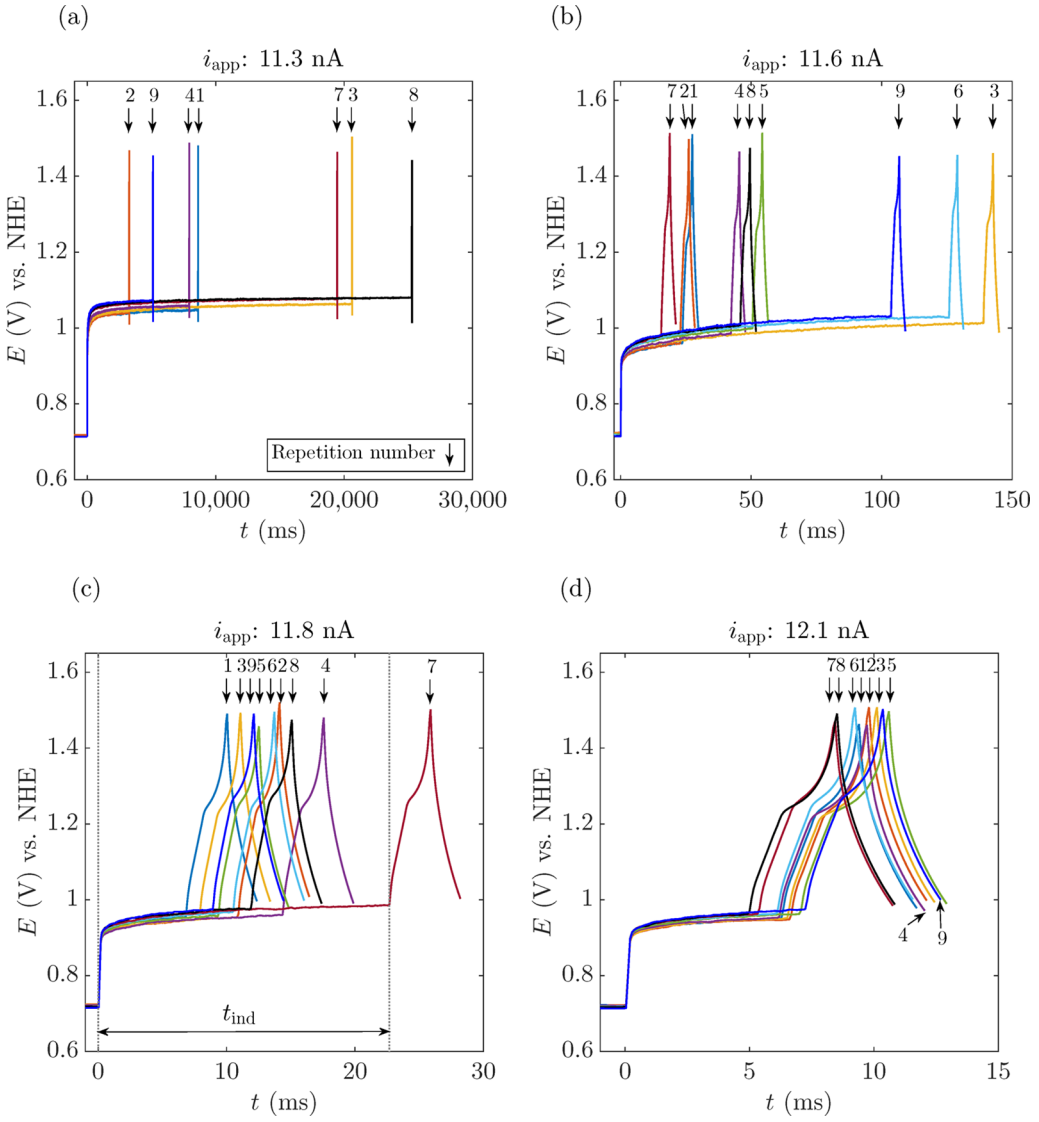

Figure 7. Potential−time measurements to determine the time needed to nucleate an O_2 nanobubble. Each panel shows a different $i_{app} < i_{nb}^{P} = 12.2$ nA and is presented on a different time scale. The electrode was 41 nm in radius. In some repetitions, for the lowest i_{app}, bubble nucleation did not occur within 30 s; therefore, the process was manually stopped. Panel (c) illustrates the interval in which the nucleation time, t_{ind}, is measured, from the moment in which the current is applied until the moment in which the nanobubble nucleates (indicated by a sudden increase in the voltage as the bubble blocks the surface of the nanoelectrode). The arrows indicate the cycle number.

Assuming Fickian diffusion on a planar disk electrode, we can relate the steady-state current i to the local concentration of O_2 being produced at the electrode surface, $C_{O_2}^{surface}$:[21,22,35]

$$i = 4nFD_{O_2}a(C_{O_2}^{surface} - C_{O_2}^{bulk}) \quad (3)$$

In eq 3, $n = 2$ is the number of exchanged electrons per molecule of O_2 generated, $F = 96\,485$ C/mol is Faraday's constant, $D_{O_2} = 1.67 \times 10^{-9}$ m^2/s is the diffusivity of O_2,[38] and $C_{O_2}^{surface}$ and $C_{O_2}^{bulk}$ are the O_2 concentrations locally at the surface of the electrode and in the bulk, respectively. $C_{O_2}^{bulk}$ is approximately zero compared to $C_{O_2}^{surface}$ in our experiments. Applying Henry's law, we can relate this supersaturated concentration at the electrode surface to P_s and therefore[35]

$$J = J_0 e^{-16\pi\gamma^3\phi(\theta)/3kT\left(\frac{i}{K_H 4nFD_{O_2}a} - P_0\right)^2} \quad (4)$$

where $K_H = 1.283 \times 10^{-5}$ mol/m^{3}Pa is Henry's constant for O_2.[39] Equation 4 can be rewritten as

$$\ln\left(\frac{J_0}{J}\right) = B\left(\frac{i}{K_H 4nFD_{O_2}a} - P_0\right)^{-2} \quad (5)$$

where $B = 16\pi\gamma^3\phi(\theta)/3kT$ and J_0 are calculated as best-fit parameters. Figure 9 shows experimentally measured nucleation rates vs the bracketed expression in eq 5 for three different electrodes, indeed displaying the linear behavior suggested by this equation. From the slope B, we can extract the contact angle θ. See below.

The nucleation rate is related to the activation energy E_a of a nanobubble nucleation by Arrhenius' law.[32] Therefore, we can achieve a one-to-one relation between both physical magnitudes:[29]

DOI: 10.1021/acs.langmuir.8b01372
Langmuir 2018, 34, 7309−7318

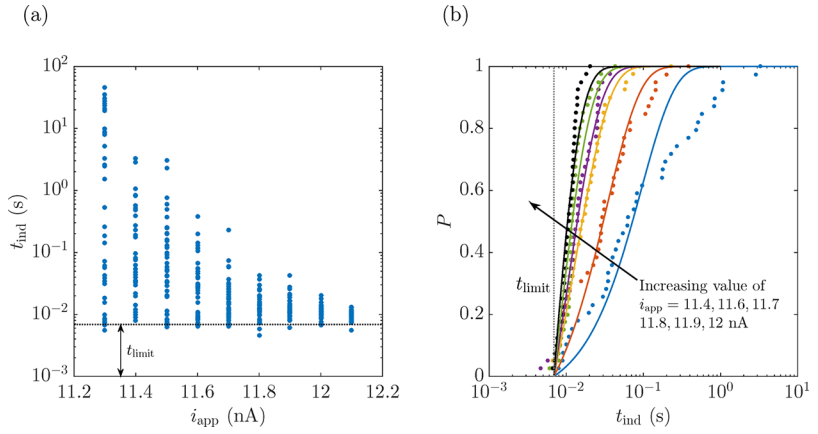

Figure 8. (a) Experimentally measured t_{ind} for different i_{app} values on a 41-nm-radius Pt electrode. (b) Corresponding cumulative probability P of a nanobubble nucleation event for i_{app} = 11.4, 11.6, 11.7, 11.8, 11.9, and 12 nA (other currents have similar results but are not shown, aiming for clarity in the figure). The theoretical curves correspond to the best fit of eq 1 to the data. The curves become increasingly vertical with increasing i_{app}: the higher the current, the higher the nucleation rate J.

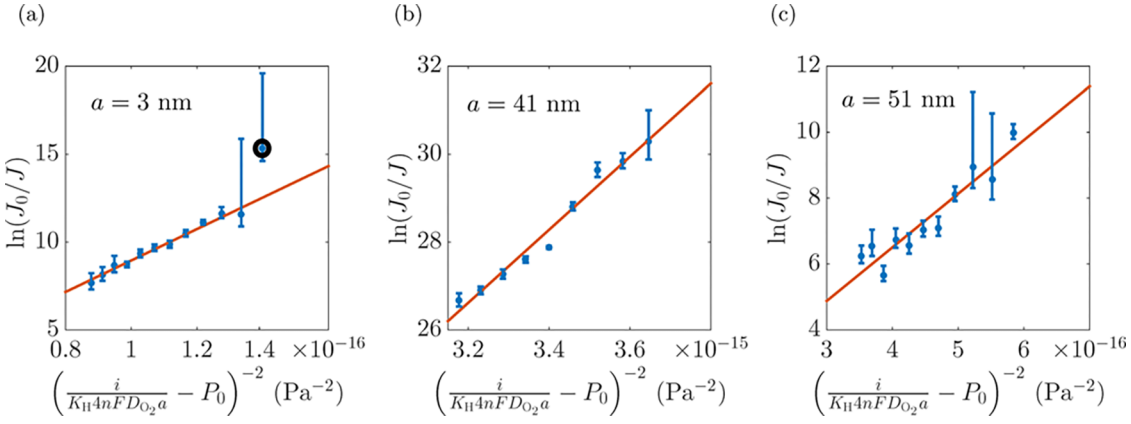

Figure 9. Logarithmic linear relation between nucleation rate J and the inverse of the squared supersaturated pressure difference for (a) a = 3 nm, (b) a = 41 nm, and (c) a = 51 nm. An outlier in (a) has been indicated by a black circle.

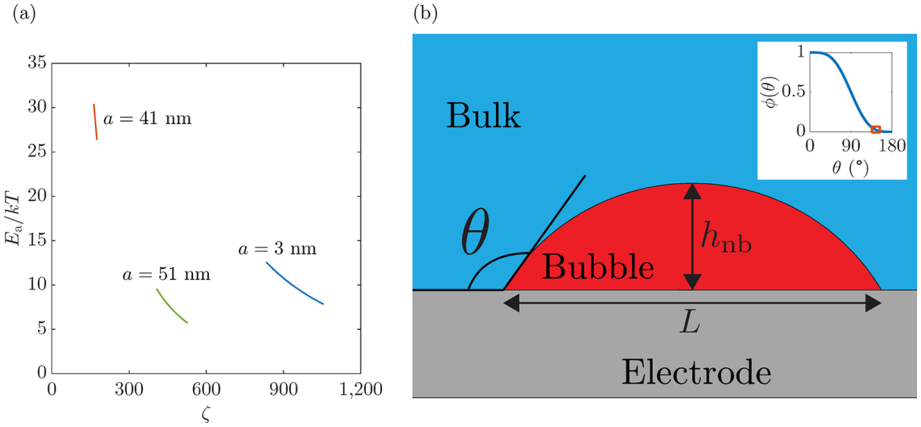

Figure 10. (a) Activation energy, E_a, as a function of the supersaturation, ζ, at different electrodes. E_a decreases with increasing i, i.e., increasing ζ. (b) Sketch of a surface nanobubble nucleus under the assumption of a spherical cap shape. The contact angle, θ, is defined on the water side, where h_{nb} corresponds to the nucleus height and L determines the nucleus footprint. Inset: geometric relation $\phi(\theta) = (1 + \cos(\theta))^2(2 - \cos(\theta))/4$ needed for the calculation of the nucleus volume assuming a spherical cap shape. The framed region indicates the domain in which all of the nanobubbles studied in this article are situated.

$$E_a = \frac{16\pi\gamma^3\phi(\theta)}{3\left(\frac{i}{K_H 4nFD_{O_2}a} - P_0\right)^2} = \frac{BkT}{\left(\frac{i}{K_H 4nFD_{O_2}a} - P_0\right)^2} \quad (6)$$

E_a thus decreases with increasing current; i.e., E_a decreases with increasing supersaturation $\zeta = (c_s - c_0)/c_0$, where c_s and c_0 refer to the O_2 concentration at supersaturation and under ambient conditions. These concentrations are related to pressure by

DOI: 10.1021/acs.langmuir.8b01372
Langmuir 2018, 34, 7309−7318

Table 1. Fitting Parameters B and J_0 in Equation 5, Activation Energy E_a from Equation 6, and Supersaturation ζ at Bubble Nucleation from Equation 7 for Different Electrodes[a]

a(nm)	B(Pa^2)	ln(J_0s)	E_a/kT	ζ
3	9.0 ± 1.0 × 10^{16}	14.3 ± 1.1	12.5 − 7.9 ± 1.2	835−1050
41	8.3 ± 1.3 × 10^{15}	32.2 ± 4.2	30.3 − 26.4 ± 4.2	160−175
51	1.6 ± 0.5 × 10^{16}	12.1 ± 2.1	9.5 − 5.7 ± 2.1	410−525

[a]The tolerances in B, J_0s, and E_a/kT indicate the error measurement when fitting Equations 5 and 6. The intervals shown in ζ represent the calculated supersaturation level at the different applied currents for each electrode.

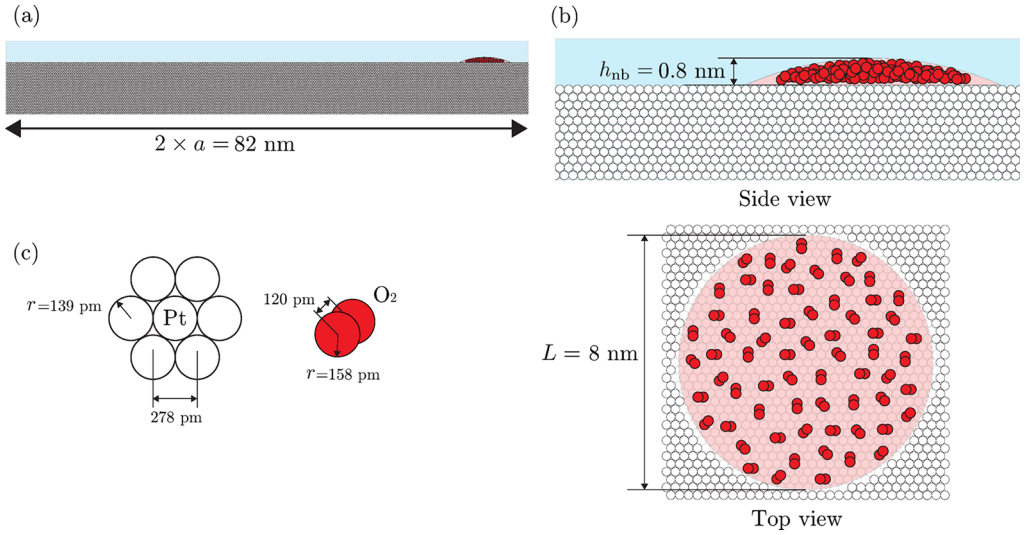

Figure 11. (a) Scale drawing[41] of a nanobubble nucleus at an a = 41 nm electrode. The white circles (best seen in panel (b)) represent Pt atoms, whereas the red ones represent O atoms. The molecular structure is defined in detail in panel (c). The close-up view of the area covered by the nanobubble nucleus is depicted from the top and the side in panel (b). The nucleus (as shown) initially covers a very small portion of the electrode surface before growing and blocking the majority of the electrode. The volume occupied by the O_2 molecules contained in the nucleus is small compared to the total nucleus volume, which may suggest that the nucleus shape may be deformed by the disjoining pressure.[37]

Henry's law at constant temperature, thus ζ can be rewritten as the pressure difference, $\zeta = (P_s - P_0)/P_0$. Associating this definition with eqs 2 and 4, we obtain an expression for the supersaturation level at the nucleation time for a bubble:

$$\zeta = \frac{i}{K_H P_0 4nFD_{O_2} a} - 1 \tag{7}$$

The different E_a values for different electrodes are represented in Figure 10a vs the corresponding levels of ζ achieved at different i_{app} values and tabulated in Table 1. As expected, the increase in supersaturation causes a decrease in the activation energy for every case.

From Figure 10a, there is no apparent relation between the different values of the activation energy E_a and the apparent radius of the electrode a nor is there a clear relation between a and fitting parameters B and J_0, as indicated in Table 1.

As mentioned above, the contact angle θ can be calculated from the slope B, namely, by the implicit equation:

$$B = \frac{16\pi\gamma^3}{3kT}\phi(\theta) = \frac{4\pi\gamma^3}{3kT}(1 + \cos(\theta))^2(2 - \cos(\theta)) \tag{8}$$

For all the different electrodes, θ ranges from 135 to 155° (inset in Figure 10b), similar to the case of H_2 nanobubbles.[29] The radius of curvature of the nucleus for an O_2 nanobubble has been reported to be r_{nb} = 10 nm,[21,22,40] which implies a Laplace pressure of $P_{nb} = 2\gamma/r_{nb}$ = 14.2 MPa. The extremely high pressure within the nanobubble justifies the surprisingly high supersaturation levels achieved locally around it at nucleation. Knowing r_{nb} and θ, the nanobubble nucleus geometry is fully determined, assuming a spherical cap shape[22,33,40] (Figure 11 and Table 2).

Table 2. Geometrical Dimensions of Different Nanobubble Nuclei[a]

a(nm)	i_{nb}^P(nA)	θ(deg)	L(nm)	h_{mb}(nm)	n_{nb}
3	5.3	144 ± 12	11.4 ± 3.2	2.0 ± 1.2	550−900
41	12.1	156 ± 1	4.1 ± 1	0.9 ± 0.0.1	50−85
51	45	151 ± 2	4.8 ± 0.3	1.2 ± 0.0.1	100−170

[a]Apparent electrode radius, a; peak current, i_{nb}^P; contact angle, θ; nucleus footprint, L; nucleus height, h_{nb}; and number of O_2 molecules in the nucleus, n_{nb}. The tolerances are the standard deviations which are derived from the calculation of the contact angle, θ, from fitting parameter B.

From the small size of the bubble nucleus footprint, L, when compared to the elctrode radius, a (Table 2), we conclude that the nanobubble nucleus covers a very small portion of the electrode. There is one exception to this case: a = 3 nm. In this particular case, the nucleus of the nanobubble is larger than the electrode. This result has several possible origins: either the nucleus is attached to some irregularities on the nanoelectrode surface, i.e., the electrode has a very nonflat surface, or the Pt disk is recessed within the glass seal,[42] providing an apparent radius determined volumetrically to be much smaller than the actual electrode size, or the disjoining pressure within the

DOI: 10.1021/acs.langmuir.8b01372
Langmuir 2018, 34, 7309−7318

nanobubble deforms its shape in a high manner such that the assumption of a spherical cap is no longer applicable. On the other hand, the total volume occupied by the number of molecules contained in the nuclei (~50−900) is small compared to the presumed initial bubble volume. From the drawing to scale in Figure 11, we can appreciate this fact: within the nanobubble nucleus volume, there is empty space which cannot be occupied by the number of molecules present. This may result in a deformed shape of the nanobubble nucleus due to the disjoining pressure.[37] From our results in Tables 1 and 2, we can conclude that there is a direct relationship between the supersaturation level ζ and the number of molecules in the nucleus n_{nb}. However, there is no apparent relation between n_{nb} and i^{P}_{nb} nor a. This issue can be due to the electrode surface properties and especially the surface chemistry that applies to the electrode during its conditioning to achieve reproducible results.

CONCLUSIONS

The nucleation of single O_2 nanobubbles at a Pt nanoelectrode has been studied in detail. The importance of surface chemistry has been exposed throughout all of this research. The necessary treatment of the Pt surface to generate a reproducible peak current i^{P}_{nb} at which nanobubbles are formed is of extreme importance if good stochastic results are to be obtained concerning the nucleation rate of nanobubbles (the corresponding analysis for a non-preconditioned electrode can be found in section 4 in the Supporting Information). In a region very close to i^{P}_{nb}, the nucleation time t_{ind} rapidly changes with a small variation on the order of tenths of a nA in the applied current i_{app}. The nucleation rate $J(i_{app})$ can be calculated from the different induction times for bubbles to nucleate when i_{app} is fixed at a certain level below i^{P}_{nb}. The Classical Nucleation Theory (eq 2) provides an accurate mathematical expression for J. Because of stochasticity, the nucleation time can vary for the same i_{app} within 2 orders of magnitude. The higher the i_{app}, the higher the supersaturation ζ and consequently the higher the nucleation rate. ζ values are large in an area local to where the nanobubble nucleates, which results from the high Laplace pressure of the nanobubble nucleus due to its small radius. From the different measured J at different ζ, the activation energies E_a have been derived along with the contact angle θ between the bubble and the electrode surface if the geometry of the nucleus of the nanobubble is approximated as a spherical cap. We can estimate the number of O_2 molecules contained in the critical bubble nucleus, which is higher for higher ζ; i.e., the more molecules are locally produced, the more molecules will form the nanobubble nucleus. Though disjoining pressure may affect the nanobubble final shape,[37] for the scope of this research the assumption of a spherical cap is more than justified since the disjoining pressure barely cause the bubble shape to deviate from a spherical cap.

ASSOCIATED CONTENT

Supporting Information

The Supporting Information is available free of charge on the ACS Publications website at DOI: 10.1021/acs.langmuir.8b01372.

Fabrication of nanoelectrodes. Nanoelectrode conditioning. Nucleation rate measurements for additional values of i_{app} and electrodes. Bubble nucleation measurements without electrode surface conditioning. (PDF)

AUTHOR INFORMATION

Corresponding Authors

*E-mail: a.morenosoto@utwente.nl.
*E-mail: d.lohse@utwente.nl.
*E-mail: white@chem.utah.edu.

ORCID

Álvaro Moreno Soto: 0000-0002-9810-7759
Hang Ren: 0000-0002-9480-8881
Detlef Lohse: 0000-0003-4138-2255
Martin A. Edwards: 0000-0001-8072-361X
Henry S. White: 0000-0002-5053-0996

Notes

The authors declare no competing financial interest.

ACKNOWLEDGMENTS

This work was supported by The Netherlands Centre for Multiscale Catalytic Energy Conversion (MCEC), an NWO Gravitation program funded by the Ministry of Education, Culture and Science of the government of The Netherlands. Nanobubble research in the White Research Group is funded by the Office of Naval Research (N00014-16-1-2541).

REFERENCES

(1) Peng, H.; Birkett, G. R.; Nguyen, A. V. Progress on the surface nanobubble story: What is in the bubble? Why does it exist? *Adv. Colloid Interface Sci.* **2015**, *222*, 573−580.

(2) Lohse, D.; Zhang, X. Surface nanobubbles and nanodroplets. *Rev. Mod. Phys.* **2015**, *87*, 981−1035.

(3) Craig, V. S. J. Very small bubbles at surfaces − the nanobubble puzzle. *Soft Matter* **2011**, *7*, 40−48.

(4) Li, M.; Tonggu, L.; Zhan, X.; Mega, T. L.; Wang, L. Cryo-EM visualization of nanobubbles in aqueous solutions. *Langmuir* **2016**, *32*, 11111−11115.

(5) Wang, L.; Wang, X.; Wang, L.; Hun, J.; Wang, C. L.; Zhao, B.; Zhang, X.; Tai, R.; He, M.; Chen, L.; Zhang, L. Formation of surface nanobubbles on nanostructured substrates. *Nanoscale* **2017**, *9*, 1078−1086.

(6) Ma, W.; Hu, K.; Chen, Q.; Zhou, M.; Mirkin, M. V.; Bard, A. J. Electrochemical size measurement and characterization of electrodeposited platinum nanoparticles at nanometer resolution with Scanning Electrochemical Microscopy. *Nano Lett.* **2017**, *17*, 4354−4358.

(7) Verhaart, H. F. A.; de Jonge, R. M.; van Stralen, S. J. D. Growth rate of a gas bubble during electrolysis in supersaturated liquid. *Int. J. Heat Mass Transfer* **1980**, *23*, 293−299.

(8) Somorjai, G. A.; Li, Y. *Introduction to Surface Chemistry and Catalysis*, 2nd ed.; John Wiley and Sons: Hoboken, NJ, 2010.

(9) Dapkus, K. V.; Sides, P. J. Nucleation of electrolytically evolved hydrogen at an ideally smooth electrode. *J. Colloid Interface Sci.* **1986**, *111*, 133−151.

(10) Velmurugan, J.; Noël, J.-M.; Nogala, W.; Mirkin, M. V. Nucleation and growth of metal on nanoelectrodes. *Chem. Sci.* **2012**, *3*, 3307−3314.

(11) Ying, Y.-L.; Hu, Y.-X.; Gao, R.; Yu, R.-J.; Gu, Z.; Lee, L. P.; Long, Y.-T. Asymmetric nanopore electrode-based amplification for electron transfer imaging in live cells. *J. Am. Chem. Soc.* **2018**, *140*, 5385−5392.

(12) Lubetkin, S.; Blackwell, M. The nucleation of bubbles in supersaturated solutions. *J. Colloid Interface Sci.* **1988**, *126*, 610−615.

(13) Hampton, M. A.; Nguyen, A. V. Nanobubbles and the nanobubble bridging capillary force. *Adv. Colloid Interface Sci.* **2010**, *154*, 30−55.

(14) Forest, T. W.; Ward, C. A. Effect of a dissolved gas on the homogeneous nucleation pressure of a liquid. *J. Chem. Phys.* **1977**, *66*, 2322−2330.

DOI: 10.1021/acs.langmuir.8b01372
Langmuir 2018, 34, 7309−7318

(15) Hemmingsen, E. A. Cavitation in gas-supersaturated solutions. *J. Appl. Phys.* **1975**, *46*, 213−218.
(16) Wilt, P. M. Nucleation rates and bubble stability in water-carbon dioxide solutions. *J. Colloid Interface Sci.* **1986**, *112*, 530−538.
(17) Pan, G.; Yang, B. Effect of surface hydrophobicity on the formation and stability of oxygen nanobubbles. *ChemPhysChem* **2012**, *13*, 2205−2212.
(18) Maheshwari, S.; van der Hoef, M.; Zhang, X.; Lohse, D. Stability of surface nanobubbles: a molecular dynamics study. *Langmuir* **2016**, *32*, 11116−11122.
(19) Rubin, M. B.; Noyes, R. M. Thresholds for nucleation of bubbles of N_2 in various solvents. *J. Phys. Chem.* **1992**, *96*, 993−1000.
(20) German, S. R.; Edwards, M. A.; Chen, Q.; White, H. S. Laplace pressure of individual H_2 nanobubbles from pressure-addition electrochemistry. *Nano Lett.* **2016**, *16*, 6691−6694.
(21) Ren, H.; German, S. R.; Edwards, M. A.; Chen, Q.; White, H. S. Electrochemical generation of individual O_2 nanobubbles via H_2O_2 oxidation. *J. Phys. Chem. Lett.* **2017**, *8*, 2450−2454.
(22) German, S. R.; Edwards, M. A.; Chen, Q.; Liu, Y.; Luo, L.; White, H. S. Electrochemistry of single nanobubbles. Estimating the critical size of bubble-forming nuclei for gas-evolving electrode reactions. *Faraday Discuss.* **2016**, *193*, 223−240.
(23) Katsounaros, I.; Schneider, W. B.; Meier, J. C.; Benedikt, U.; Biedermann, P. U.; Auer, A. A.; Mayrhofer, K. J. J. Hydrogen peroxide electrochemistry on platinum: towards understanding the oxygen reduction reaction mechanism. *Phys. Chem. Chem. Phys.* **2012**, *14*, 7384−7391.
(24) Lubetkin, S. D. Why is it much easier to nucleate gas bubbles than theory predicts? *Langmuir* **2003**, *19*, 2575−2587.
(25) MacInnes, D. A. The mechanism of the catalysis of the decomposition of hydrogen peroxide by colloidal platinum. *J. Am. Chem. Soc.* **1914**, *36*, 878−881.
(26) Garwig, P. L. *Heterogeneous Decomposition of Hydrogen Peroxide by Inorganic Catalysis*; PN: 1966.
(27) Chen, Q.; Wiedenroth, H. S.; German, S. R.; White, H. S. Electrochemical nucleation of stable N_2 nanobubbles at Pt nanoelectrodes. *J. Am. Chem. Soc.* **2015**, *137*, 12064−12069.
(28) Svetovoy, V. B.; Sanders, R. G. P.; Elwenspoek, M. C. Transient nanobubbles in short-time electrolysis. *J. Phys.: Condens. Matter* **2013**, *25*, 184002.
(29) German, S. R.; Edwards, M. A.; Ren, H.; White, H. S. Critical nuclei size, rate, and activation energy of H_2 gas nucleation. *J. Am. Chem. Soc.* **2018**, *140*, 4047−4053.
(30) Brandel, C.; ter Horst, J. H. Measuring induction times and crystal nucleation rates. *Faraday Discuss.* **2015**, *179*, 199−214.
(31) Hyde, M. E.; Compton, R. G. A review of the analysis of multiple nucleation with diffusion controlled growth. *J. Electroanal. Chem.* **2003**, *549*, 1−12.
(32) Blander, M.; Katz, J. L. Bubble nucleation in liquids. *AIChE J.* **1975**, *21*, 833−848.
(33) Kashchiev, D.; van Rosmalen, G. M. Review: nucleation in solutions revisited. *Cryst. Res. Technol.* **2003**, *38*, 555−574.
(34) Butt, H.-J.; Kappl, M. Normal capillary forces. *Adv. Colloid Interface Sci.* **2009**, *146*, 48−60.
(35) Chen, Q.; Luo, L.; Faraji, H.; Feldberg, S. W.; White, H. S. Electrochemical measurements of single H_2 nanobubble nucleation and stability at Pt nanoelectrodes. *J. Phys. Chem. Lett.* **2014**, *5*, 3539−3544.
(36) Fletcher, N. H. Size effect in heterogeneous nucleation. *J. Chem. Phys.* **1958**, *29*, 572−576.
(37) Svetovoy, V. B.; Dević, I.; Snoeijer, J. H.; Lohse, D. Effect of disjoining pressure on surface nanobubbles. *Langmuir* **2016**, *32*, 11188−11196.
(38) Wakabayashi, N.; Takeichi, M.; Itagaki, M.; Uchida, H.; Watanabe, M. Temperature-dependence of oxygen reduction activity at a platinum electrode in an acidic electrolyte solution investigated with a channel flow double electrode. *J. Electroanal. Chem.* **2005**, *574*, 339−346.
(39) Tham, M. K.; Walker, R. D.; Gubbins, K. E. Diffusion of oxygen and hydrogen in aqueous potassium hydroxide solutions. *J. Phys. Chem.* **1970**, *74*, 1747−1751.
(40) Kikuchi, K.; Ioka, A.; Oku, A.; Tanaka, Y.; Saihara, Y.; Ogumi, Z. Concentration determination of oxygen nanobubbles in electrolyzed water. *J. Colloid Interface Sci.* **2009**, *329*, 306−309.
(41) Batsanov, S. S. Van der Waals radii of elements. *Inorg. Mater.* **2001**, *37*, 871−885.
(42) Chen, Q.; Luo, L.; White, H. S. Electrochemical generation of a hydrogen bubble at a recessed platinum nanopore electrode. *Langmuir* **2015**, *31*, 4573−4581.

DOI: 10.1021/acs.langmuir.8b01372
Langmuir 2018, 34, 7309−7318